Special Collection

Restructuring of Nanoporous Gold Surfaces During Electrochemical Cycling in Acidic and Alkaline Media

Alex Ricardo Silva Olaya,[a] Birthe Zandersons,[b] and Gunther Wittstock*[a]

The electrochemical behavior of nanoporous gold (NPG) obtained by dealloying a AgAu alloy has been investigated by means of cyclic voltammetry (CV) in 0.1 M H_2SO_4 and 0.1 M KOH solutions supplemented by X-ray photoelectron spectroscopy (XPS) and scanning electron microscopy (SEM) in order to understand different effects of the electrochemical treatment on the development of the surface structure of NPG. In order to reduce the *IR* drop caused by the high surface area of the bicontinuous network of pores and ligaments in NPG, NPG was transformed to a powder, from which a small portion was filled into a cavity microelectrode (CME). Additionally, this avoided sample-to-sample variation from the dealloying process because many fillings could be made from one NPG monolith. The cycling in 0.1 M H_2SO_4 led to restructuring of the surface to a more faceted one, only after the residual silver on the surface had been removed in the initial scan. The same cycling program in 0.1 M KOH did not cause restructuring. However, a transfer of the sample to 0.1 M H_2SO_4 could start the process. The ligament size did not change during restructuring. Additionally, it was found that residual Ag in NPG stabilizes the highly curved surfaces of the ligaments containing a high density of surface defects. The dissolution of the residual Ag in acid electrolytes lifts the blockage towards surface restructuring. These findings form a basis for understanding the electrochemical behavior of NPG and to devise appropriate treatments, for instance for their use in electrocatalysis.

1. Introduction

Nanoporous gold (NPG) has emerged as an interesting electrode material due to its huge surface area and metallic nature that offers high electrical conductivity.[1] The use of this material was explored for critical reactions in fuel cell technology, such as oxygen reduction,[2] hydrogen evolution[3] and carbon monoxide oxidation.[4] Moreover, NPG exhibits good performance for alcohol electrooxidation,[5,6] especially in alkaline media. NPG is obtained by selective dissolution of an alloy of Au with a less noble element.[7] In our study, NPG is prepared from a AuAg alloy. AgAu starting alloys have the particular advantage that both elements form a solid solution and have nearly identical atomic sizes. The final material always contains a small amount of the less noble metal, that is suspected to influence the (electro)catalytic behavior of NPG. As a consequence, research has been devoted to understand the behavior of the material in a fundamental way.[8,9,10]

The adjustable sizes of pores and struts (called 'ligaments') range between ten and several hundred nanometers and thus support effective mass transport in liquid phase. The change of feature sizes is enabled by (surface) diffusion of the metal atoms leading to a state of lower surface energy. Those transport processes occur as long as the activation energy for diffusion is provided[11,12] and cause a phenomenon called coarsening, because the overall shape of the structural elements is mainly preserved while the diameters of pores and ligaments grow. Coarsening occurs already during the potentiodynamic dealloying process used here. Because longer dealloying time or more potential cycles in the dealloying procedures decrease the residual Ag content but also leave more time for coarsening, the ligament diameter growths as the residual Ag content decreases.[10,13] Practically, potentiodynamic dealloying often yields a final ligament size of ca. 45 nm.[14,15] The presence of halide facilitates surface diffusion and accelerates coarsening.[16]

Thermal annealing is the most common way of enlarging pores and ligaments after dealloying.[17] During this process the content of the less noble element at the surface may change and thus impact (electro)catalysis.[18] Pulsed electrochemical etching in HCl has been demonstrated to enlarge the pore size while preserving the surface area in NPG thin films.[19] There are contradicting reports if electrochemical cycling of NPG electrodes in non-complexing solutions after the dealloying procedures can also cause further coarsening and a concomitant decrease of electrochemical active surface area A_{ECSA}. Matharu et al.[20] used cycling in 0.1 M H_2SO_4 solution for different time to systematically vary pore sizes between 20 and 150 nm in 600 nm NPG thin films. The presence of Pt in NPG obtained from a ternary AuAgPt starting alloy could stabilize small ligaments against further electrochemical coarsening.[21] While extended periods of carbon monoxide oxidation on NPG led to

[a] *A. R. Silva Olaya, Prof. Dr. G. Wittstock*
Department of Chemistry
Carl von Ossietzky University of Oldenburg
26111 Oldenburg, Germany
E-mail: wittstock@uol.de
[b] *B. Zandersons*
Institute of Materials Physics and Technology
Hamburg University of Technology
21073 Hamburg, Germany

Supporting information for this article is available on the WWW under https://doi.org/10.1002/celc.202000923

An invited contribution to a Special Collection dedicated to GDCh Electrochemistry: At the Interface between Chemistry and Physics.

coarsening of the ligaments,[4] other reports did not find an effect on the ligament size, for instance for alcohol oxidation.[5,9] As consequence, very little is known about the mechanism of coarsening and the influencing factors during electrochemical cycling on NPG.[22]

One of the first systematic studies in this area was presented by Wang et al.[23] showing that the preferential formation of specific low index crystal facets is promoted on NPG depending on the potential scan rate *v* and the number of potential cycles. The dealloying for the preparation of those NPG samples was conducted by free corrosion of a AgAu master alloy film yielding a NPG film with a residual Ag content of 1.5 at%. This result is crucial for the rational design of electrocatalysts. However, information is available for acidic media only, where NPG is less active as electrocatalyst for alcohol oxidation than in alkaline solution. The study of Wang et al.[23] appears to be in contradiction to the findings for other gold electrodes, where cycling into the potential regions of Au surface oxidation increased roughness of single crystal electrodes as evidenced by scanning tunneling microscopy.[24] More recently, Ahrens et al.[25] demonstrated that the signature of surface roughness could clearly be detected even for commonly used flat polycrystalline Au electrodes. This process could be linked to the growth of Au nanoparticles on the Au surface.

In this study, we compare the effect of electrochemical cycling of NPG in different electrolytes on the structure and composition of the surface in order to understand the fundamental behavior of the material and to enable its use in electrocatalysis for substance transformation or sensors. The observations are correlated with the nature of the electrolyte and the fate of the residual, less noble metal.

2. Results and Discussion

2.1. Filling of Cavity and Morphological Characterization of NPG

Throughout this study we used NPG obtained by an established multistep-potentiodynamic dealloying protocol in Suprapur 1 M $HClO_4$ (details in Experimental section). It involves first oxidation at fixed potentials followed by potentiodynamic cycling in 1 M $HClO_4$, during which the residual Ag mole fraction x_{Ag} in the bulk of the ligaments is decreased to ca. 1% as measured by energy-dispersive X-ray spectroscopy (EDX) while at the same time the ligament diameter increases to about 40 nm. After 2–6 weeks storage in air, the NPG monoliths are transformed to a powder. For brevity, we call this state of the NPG powder "as prepared" in this manuscript. We determined $x_{Ag} = 8\%$ at the surface of the ligaments by X-ray photoelectron spectroscopy (XPS) at this state of the sample, which is considerably higher than the bulk x_{Ag} (vide supra), which is in line with previous findings.[18] In this manuscript, we focus on changes of the surface state of this NPG material upon further electrochemical cycling experiments in 0.1 M KOH and 0.1 M H_2SO_4 in order to elucidate which changes may occur during application of NPG for electrocatalysis in sensors or energy conversion devices. The structure evolution during the dealloying process itself is not a subject of this study as it has already been thoroughly analyzed.[10,13,14]

The detailed analysis of the surface voltammograms was enabled by a cavity microelectrode (CME)[26] loaded with NPG powder. The CME consists of an encased and recessed Au wire that forms a cylindrical cavity with the glass sheath of 100 µm diameter and 30 µm depth. Figure 1A shows a scanning electron microscopy (SEM) image of the NPG sample after loading NPG powder into the CME by gently pressing it into the NPG powder. Then the powder 'cake' was transferred onto carbon tape for morphological characterization. Figure 1A reveals larger gaps between the individual NPG grains of different size. The images in Figure 1B are enlarged views obtained at different regions of the sample as marked in Figure 1A. They reveal that the porous structure is preserved and uniform after pressing the NPG sample against the tip of the microelectrode during the filling process. However, some parts of the sample in image Figure 1A seem to be flat. These are mainly those grains in direct contact with the side wall or bottom of the cavity and those that form the outer surface as evident from further images in the Supporting Information (SI),

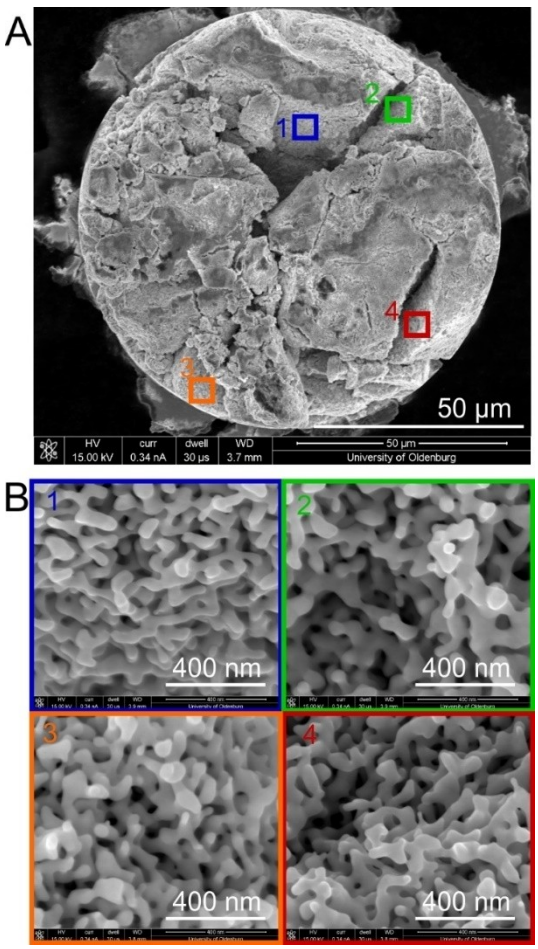

Figure 1. SEM images of NPG sample transferred from the CME. A) Top view of the sample transferred to the carbon tape. B) Morphology of the grains in four different zones. The zones are marked by numbers and colored squares in (A). The squares are not to scale.

Figure S1. The deformation is due to the pressure exerted during filling of the cavity; however, the affected area is negligible compared to the unaffected electrochemically active surface area A_{ECSA} of the porous electrode. This fact can also be established qualitatively from Figure 1A, where the porous parts of the sample dominate the outer surface. A magnified image in Figure S1B suggests a more compact structure of the deformed zones, i.e. a decreased porosity. However, even those surface regions are still far from being flat.

The measured A_{ECSA} can be compared to the value that would result from the ideal filling of the CME (by an ingot matching exactly the geometric shape of the cavity as depicted in Figure S2. The expected $A_{ECSA} = 0.139\ cm^2$ (SI-2) is obtained from the specific surface area of $11.8\ m^2 g^{-1}$ of the used NPG, the dimension of the used cavity obtained from confocal laser scanning microscopy (see experimental). The experimental value $A_{ECSA} = 0.145\ cm^2$ was determined by integration of the cathodic peak of the cyclic voltammogram (CV) in Figure 2, curve 2 and the specific charge of 390 $\mu C\,cm^{-2}$ for the reduction of surface gold oxide.[27] The comparison to the value from a pure geometric consideration illustrates that the slight overfilling has a stronger influence then the unavoidable voids for which an example is visible below the blue rectangle in Figure 1A.

The average ligament diameter amounts to 40 nm calculated from averaging the diameter of 20 measured ligaments in each of the images in Figure 1B. Details of this procedure are documented SI-3. This obtained mean diameter agrees with previous reports for this dealloying process.[28]

The use of the CME brings several advantages for the electrochemical characterization of NPG. First of all, many samples can be prepared from one and the same monolith. Their CVs differ slightly in the overall currents due to different loading. After normalization to A_{ECSA}, the voltammetry is highly reproducible, a fact that is much more difficult to prove when using a new NPG monolith for each CV. The work with aliquots of *one* powdered NPG monolith also facilitates a much higher throughput in experimentation and resulted in higher reproducibility. The greatly reduced overall currents are a further advantage of using a CME compared to macroscopic monolithic NPG samples because smaller currents cause a smaller *IR* drop and reduce the associated artefacts in voltammetry. The high resolution of voltammetric peaks shown below was impossible to achieve in our hands with macroscopic NPG samples.

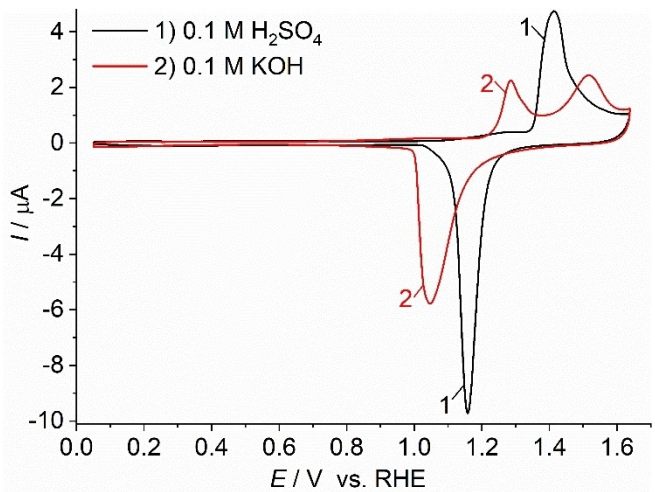

Figure 2. CV of NPG in 1) 0.1 M H_2SO_4 and 2) 0.1 M KOH; $v = 10\ mV\,s^{-1}$.

2.2. Overview of the Electrochemical Behavior in H_2SO_4 and KOH

Figure 2 compares the initial CVs of as prepared NPG in 0.1 M H_2SO_4 and in 0.1 M KOH. In H_2SO_4, the behavior is merely capacitive between 0.05 V and approx. 1.00 V, where the NPG surface remains metallic. Surface oxidation-reduction processes take place between 1.00 V and 1.64 V. There is a pre-oxidation signal between 1.00 V and 1.32 V with a maximum at 1.29 V, followed by a single broad anodic peak with a maximum at 1.41 V. This single anodic signal has been reported previously for highly rough and disordered gold surfaces obtained after etching with Ar^+.[29] The pre-oxidation signal has neither been described before for NPG nor for other highly rough surfaces.[25] The somewhat similar surface electrochemistry of NPG (Figure 1) and intentionally roughened surfaces in Refs. [25] and [29] is plausible when considering that the highly curved surface of individual ligaments in NPG is dominated by step and kink defects that truncate the metal crystal at the surface. The potential scan is reversed at the so-called Burshtein minimum,[30] at which one oxide monolayer is formed and a further current increase due to water oxidation or oxide multilayer formation has not started yet. The subsequent negatively going scan shows a symmetrical peak centered near 1.15 V, which is associated with the reduction of the gold oxide monolayer.

In 0.1 M KOH solution, the capacitive zone is restricted to 0.05 V to 0.60 V and thus narrower than in 0.1 M H_2SO_4 solution. Please note, that the potential scale is already transformed to RHE so that obvious pH effects are corrected. The surface redox waves are found between 0.60 V and 1.64 V. The Burshtein minimum is reached at 1.64 V,[31] exactly at the same value as in 0.1 M H_2SO_4, which suggests that the oxide monolayer formation does not depend on the pH. A pre-oxidation zone appears between 0.70 V and 1.16 V. Borkowska et al.[32] have observed this signal on flat polycrystalline gold and related it to the chemisorption of OH^- that involves a partial charge transfer. The signal has also been reported by Hamelin et al.[31] for single crystal gold electrodes before. Along the positively going scan, there are an anodic peak at 1.29 V followed by the shoulder at 1.33 V and a second anodic peak at 1.52 V. The negatively going scan shows an asymmetrical reduction peak between 1.40 V and 0.70 V. The reduction current rises slowly until it reaches the maximum reduction current at 1.05 V. Afterwards, the reduction current drops to reach the inflexion point at 0.99 V. There is not much literature available regarding the behavior of gold with an enhanced roughness in alkaline media.[33] However, some studies with gold nanoparticles in alkaline media[34,35] showed that the electrochemical behavior of the nanoparticles

is similar to that of polycrystalline Au of low roughness. In the case of NPG, the anodic peak at 1.52 V and the asymmetry of the cathodic peak show that this surface does not behave simply as a polycrystalline gold electrode of enormous surface area. In particular, the anodic peak at 1.52 V neither appears in voltammograms of single crystal, polycrystalline nor of nanoparticulate Au electrodes. We hypothesize that this signal is associated with the residual Ag content in NPG after the dealloying process and therefore does not occur in the other forms of rough gold electrodes. Further evidence will be provided below.

2.3. Stability During Extended Potential Cycling in H_2SO_4

In order to evaluate the stability of the surface, NPG was cycled 100 times in both, 0.1 M H_2SO_4 and 0.1 M KOH, between 0.05 V and the Burshtein minimum. Figure 3 shows the results in 0.1 M H_2SO_4. During the first four cycles the voltammograms changes dramatically. Especially the broad signal between 1.0 V and 1.32 V in the first potential cycle disappears in subsequent cycles. Due to the low potential, this signal may be related to the oxidation of Ag species at the surface of ligaments and the surface oxidation of highly curved zones of the ligaments. Oxidized Ag species will dissolve in an acidic electrolyte and the defect-rich surface is susceptible to change (vide infra). Hence, the broad signal between 1.0 V and 1.32 V is only visible in the first cycle in acidic electrolytes. The onset potential for surface oxidation shifts from 1.32 V to 1.23 V and multiple peaks develop between 1.23 V and 1.65 V. During the third potential cycle the anodic peak current at 1.36 V grows, and a peak at 1.38 V is resolved. The peak in the second cycle at 1.42 V disappears and becomes a minimum in the third cycle. A decrease is also observed for the cathodic peak area from the first to the subsequent potential cycles. Integration of the anodic Q_a and cathodic charges Q_c shows that the ratio Q_a/Q_c is 1.17 for the first cycle. This ratio is unity (0.999 ± 0.003) for the 2nd to 14 cycle. Indicating an additional oxidative process in the

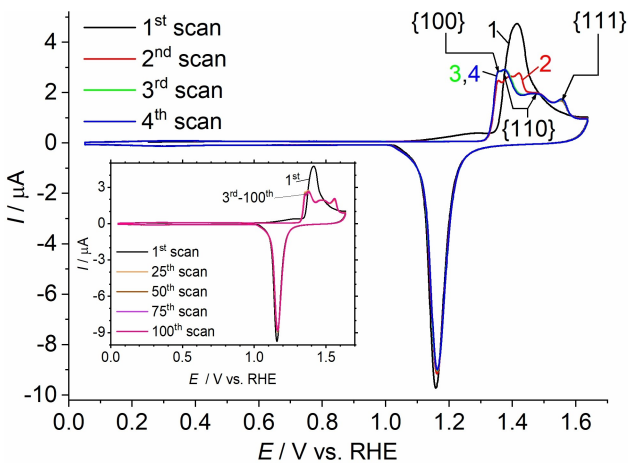

Figure 3. Continuous cycling of NPG in 0.1 M H_2SO_4 at $v = 10$ mV s^{-1}. The main graph shows the first four cycles and the inset compares the evolution of every 25th cycle to the 1st one.

first positively going scan that is not reverted in the subsequent negatively going scan.

From the third scan onward, the general shape of the voltammogram does not change. The multiple peaks observed in the region of surface oxidation are characteristic for polycrystalline Au electrodes with low index single crystal terraces, which suggest the formation of facets or wider surface domains such as {100} at 1.35 V, {110} at 1.38 V and 1.48 V, as well as {111} at 1.55 V.[31] Over prolonged cycling, the peaks decrease with cycling, except the one at 1.56 V which grows with cycling (Figure 3, inset). The oxide formation signal in Figure 3, curve 4 can be described by seven overlapping Gaussian contributions (Figure S4B). Each component has contributions from several index planes. A very caution assignment of the signals to dominating low index planes, provides an estimate that about 24% of the surface atoms are located in (100) planes and 23% in (111) planes. The remaining part of the oxide formation signal are caused by divers highly stepped surfaces, whose signal overlap and also include the signal from the (110) facet. It is exactly this signal, which decreases fastest while those of (100) and (111) increase. Please also note the discussion on the limitations of such a procedure in SI-4.

The change per cycle is continuously decreasing over the entire experiment. In general, similar surface restructuring processes have been observed for prolonged cycling of flat polycrystalline Au electrodes.[25] However, the trends are much more pronounced for NPG, possibly because of the higher density of easily oxidable defects on an extended surface that dissolve into the electrolyte solution at the positive limit of the potential excursion[36] and are re-deposited by reduction on the energetically more stable facets during the negatively going scan. Wang et al.[23] suggested that cycling promotes a reorganization of the as-prepared, defect-rich surface of NPG to a more stable surface structure with larger regions of low index facets. Interestingly, at low scan rate, {111} terraces were favored; but at high scan rate, {100} terraces were formed.[23] While rearrangement of surface atoms, which is undoubtedly required for such changes to occur, suggests a concomitant coarsening of the NPG structure, SEM images obtained before and after potential cycling could not confirm this notion.[23] Instead, ligament and pore sizes remain roughly constant.[23]

Figure 4 shows SEM images of three different zones of the sample before (A, B, C) and after (A′, B′ C′) electrochemical cycling 0.1 M H_2SO_4. The porous structure is clearly resolved in these images. After cycling, the porous structure is less compact. The result indicates that the morphology of NPG changes, but this change differs from the changes during thermal annealing,[12] in which pore and ligament sizes increase simultaneously while preserving the general shape of the ligaments. This can be rationalized as a transition from initially cylindrical shape of the ligaments with a high density of defects to a prismatic shape with a lower density of surface defects but essentially unchanged diameter. The suggested changes are depicted in Scheme 1.

An interesting observation can be made by first cycling the sample in 0.1 M H_2SO_4 and then transferring it to 0.1 M KOH for characterization. The CV in 0.1 M KOH (Figure 5, curve 2) shows

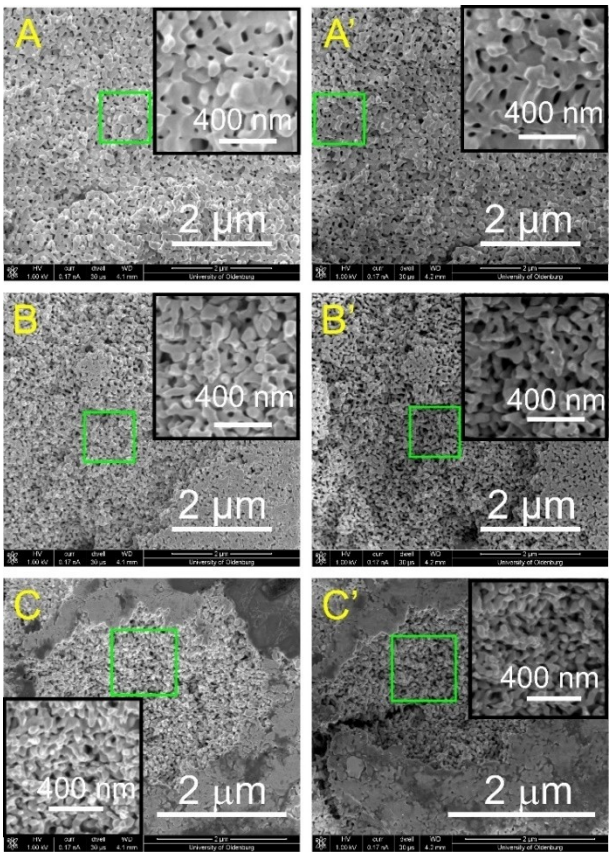

Figure 4. Characterization of NPG sample by SEM. Three different zones of the same sample are depicted. a, b, and c correspond to the sample before to be cycled and a′, b′ and c′ correspond to the same zones after cycling. The insets show an enlarged view of the areas marked by the green rectangles.

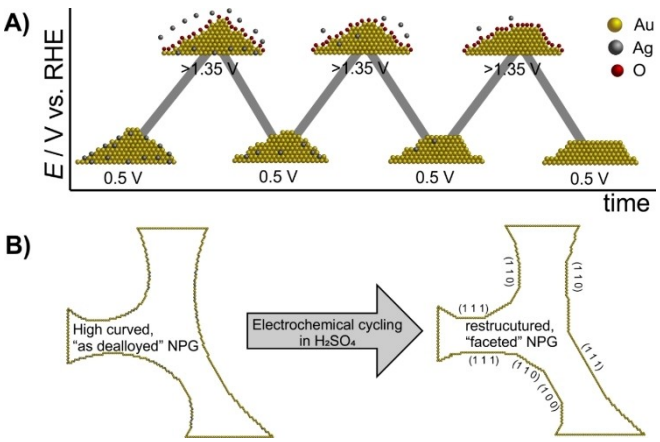

Scheme 1. Change of ligament geometry during potential cycling in H_2SO_4 solution. A) Restructuring process of the surface on the atomic level. The spheres represent Au, Ag and O surface atoms. B) Development of the ligament geometry during potential cycling in 0.1 M H_2SO_4.

major differences to the voltammogram obtained in the same electrolyte before cycling in sulfuric acid (Figure 2, curve 2). For a convenient comparison, both curves are replotted in Figure S5 in one diagram. The surface oxidation starts at lower potentials,

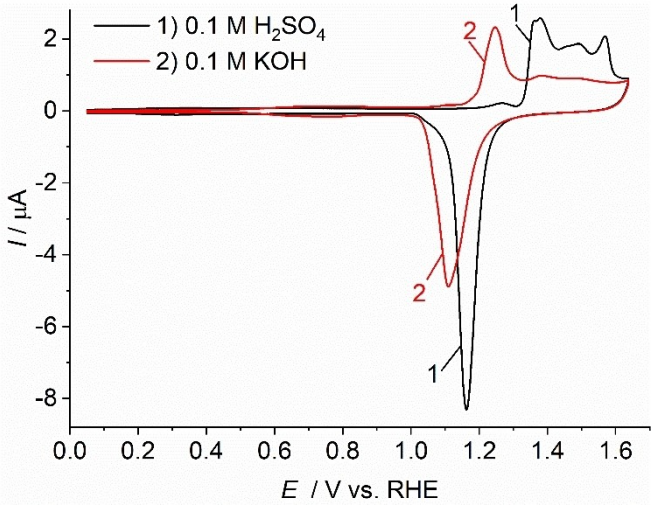

Figure 5. CV of NPG after 100 potential cycles in 0.1 M H_2SO_4 and transfer to 1) 0.1 M H_2SO_4 and 2) 0.1 M KOH; $v = 10\ mV\,s^{-1}$.

the cathodic peak is shifted to more positive potentials and the cathodic peak assumes a more symmetrical shape. These observations suggest that oxidation is easier and more reversible after NPG has been cycled 100 times in H_2SO_4. The peak at 1.52 V in Figure 2, curve 2 deserves particular attention, because it is *completely absent* in the voltammogram in KOH in Figure 5, curve 2. The voltammogram in KOH obtained after cycling in H_2SO_4 is closer to reported voltammograms for polycrystalline Au electrodes and Au nanoparticles.[34] This observation reinforces the hypothesis that the as prepared NPG surface before restructuring is completely different from the surface of other gold electrodes. As mentioned before, a cyclic voltammogram with the peak at 1.52 V, as obtained in 0.1 M KOH before cycling (Figure 2, curve 2), has never been reported for any gold electrode to the best of our knowledge. This fact suggests that the peak at 1.52 V is related to the special surface structure and composition of NPG. Those features likely comprise a high density of surface defects, a small size of crystal facets, and residual silver species that may be essential for stabilizing them. At pure Ag electrodes, transition from Ag^{I} to Ag^{II} species have been reported at this potential.[37] Whether this transition does also occur for residual Ag dispersed in an Au matrix of NPG, cannot be confirmed from voltammetric data alone. We note a very stable behavior of the electrodes cycled in KOH although Pourbaix diagrams of pure Ag electrodes suggest anodic dissolution of Ag^{I} species over the entire pH range.[38] It seems that Ag species dispersed in an Au matrix are much less susceptible to removal from the solid phase in alkaline solution than for pure Ag electrodes or in acidic solution. Moreover, Ag surface concentration even increases during prolonged cycling because Ag atoms from the bulk of the material become exposed to the surface (vide infra).

In order to exclude transfer artefacts, a control experiment was performed consisting of cycling in 0.1 M H_2SO_4 followed by a transfer to the same solution (0.1 M H_2SO_4) for characterization (Figure 5, curve 1). The obtained CV of NPG in 0.1 M

H_2SO_4 is identical to the last potential cycle in the inset of Figure 3. This proves the relative stability of the restructured surface even to a short exposure to ambient air.

2.4. Stability During Extended Potential Cycling in KOH

Continuous cycling in 0.1 M KOH (Figure 6) does not cause the pronounced changes, which were found during the first cycles in 0.1 M H_2SO_4 (Figure 3). In Figure 6, the peak at 1.29 V is shifted by only 20 mV to less positive potentials and becomes slightly more defined. This is an evidence that the surface structure of the NPG samples becomes more homogeneous and energetically similar. However, the CV does not develop clear peaks in KOH solution that would be indicative for the different single crystal facets. This makes it hard to diagnose a surface restructuring. This is also a consequence of the relatively close position of the signals for the surface oxidation of the three basal planes (100), (110) and (111) in alkaline media.[34]

Hernandez et al.[34] have reported that CVs of Au nanoparticles in 0.1 M KOH are very similar to those of polycrystalline Au electrodes. However, the CVs obtained for NPG are quite different from those of Au nanoparticles and polycrystalline Au. Especially the anodic signal at 1.52 V in Figure 6 does not appear in the CV of other Au electrodes. Those electrodes exhibit a symmetrical cathodic peak centered at 1.10 V for polycrystalline Au and 1.17 V for Au nanoparticles. For NPG, the cathodic peak is shifted to 1.05 V. This peak is asymmetrical indicating that the surface oxide reduction requires a larger initial driving force. However, the reduction proceeds very rapidly once the barrier has been passed. All features of the voltammogram of NPG are retained over 100 cycles including the peak at 1.52 V and the asymmetry of the cathodic peak. This corresponds to the conservation of the porous network as evident from SEM images in Figure S6. The ratio of anodic to cathodic charges Q_a/Q_c within a voltammetric cycle is always close to one, but shows a slight trend for a continuous decrease (1st cycle 1.016; 6th cycle 1.006; 14th 0.998). A slight decrease of the peak area, best visible for the cathodic peaks in the inset, can be explained by the coarsening of the ligaments. When following the explanation of Wang et al.,[23] structural changes of the sample have to take place on the surface and, therefore, are facilitated by place exchange reaction at the surface during surface oxidation and reductions cycles.

The lack of restructuring during cycling in 0.1 M KOH is more evident when the sample is transferred afterwards to 0.1 M H_2SO_4 or 0.1 M KOH for recording another CV for characterization (Figure 7). Those CVs resemble the initial voltammograms in Figure 2 that were recorded before any cycling. This demonstrate that potential cycling in 0.1 M KOH does not induce the restructuring of the ligament surface that was observed for cycling in 0.1 M H_2SO_4.

A complete explanation for the dynamic behavior of NPG not only has to involve the relaxation of the highly energetic defects on the ligament surface, but also the role of dissolution and re-deposition processes that take place at positive potentials. Especially the role of residual silver inside NPG and at its surface[18] may profoundly change the voltammetry because it is expected that Ag dissolves when oxidized in acidic media. In contrast, passivating silver oxides may form in alkaline solutions. The loss of Ag from the surface in acidic solution may then also further influence the restructuring process. This conclusion is also supported by the observation of Cherevko and Chung[39] on NPG obtained by hydrogen bubble-templated Au electrodeposition and is completely free of residual less noble metals. This material coarsens very fast and strongly in ambient air and during potential cycling in H_2SO_4.

XPS analysis was carried out for as-prepared NPG, NPG cycled 100 times in 0.1 M H_2SO_4 and NPG cycled in 0.1 M KOH (Figure 8). The intensities of the Ag 3d spectra in Figure 8 are normalized to the intensity of the Au 4f signal of the same sample. The as prepared sample exhibit a Ag mole fraction x(Ag)/ek; within the information depth of XPS as x(Ag) = 8 % [x

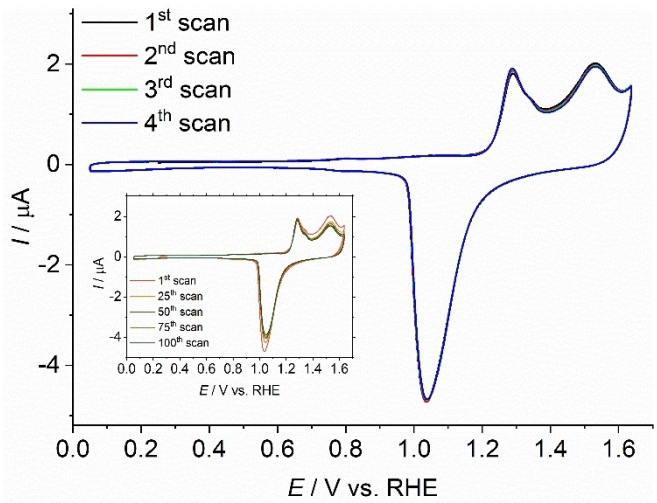

Figure 6. Continuous cycling of NPG in 0.1 M KOH at $v = 10$ mV s^{-1}. The main graph shows first four cycles and the inset compares the evolution of every 25th cycle to the 1st one. (Cycles 1–4 retrace.)

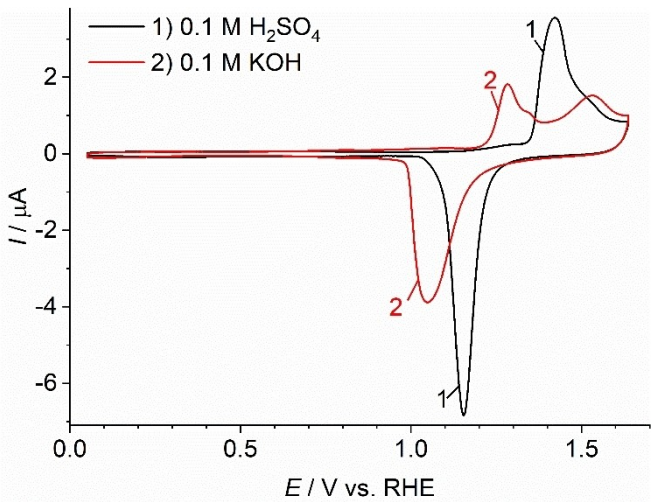

Figure 7. CV of NPG in 0.1 M H_2SO_4 (red line) and 0.1 M KOH (black line) after be cycled 100 times in 0.1 M KOH; $v = 10$ mV s^{-1}.

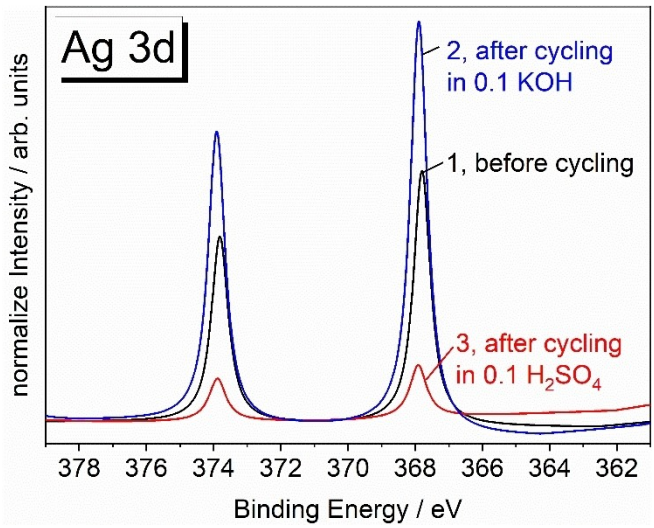

Figure 8. Ag 3d XPS of NPG samples 1) before cycling, 2) after 100 potential cycles in 0.1 M H_2SO_4, and 3) after 100 potential cycles in 0.1 M KOH.

(Au) = 92 %]. This demonstrates a strong enrichment of Ag compared to the residual Ag content in the bulk, which was 1 % as measured by EDX. This enrichment is completely in line with our recently reported findings about relative surface enrichment in thermally and electrochemically treated samples.[18] The change of the relative XPS intensity after cycling is very clear in both electrolytes. Potential cycling in 0.1 M H_2SO_4 causes dissolution of residual Ag at the surface resulting in a decrease of the Ag mole fraction x(Ag) within the information depth of XPS to x(Ag) = 2 % [x(Au) = 98 %]. This evidences a depletion of Ag at the surface of ligaments due to electrolytic Ag dissolution in acidic solution. Electrolytic dissolution does not take place in the same way in alkaline media since Ag^{I} within an Au matrix either does not leave the solid phase or forms insoluble surface layer of silver hydroxide or specifically adsorbed negatively charged hydroxo complexes that remain on the surface as adsorbed anions. This interplay of mobility of metal atoms in NPG constantly expose atoms to the interface. The higher oxophilicity of silver stabilizes Ag atoms at the surface. This leads to an Ag enrichment within the XPS information depth from x(Ag) = 8 % to x(Ag) = 13 % [x(Au) = 87 %].

If a sample is first cycled 100 times in 0.1 M KOH, then analyzed for one potential cycle in 0.1 M H_2SO_4 and then transferred back to KOH, the broad peak at 1.52 V is not observed anymore. Consequently, the Ag dissolution occurs in the broad anodic peak in the first potential cycle in sulfuric acid at 1.41 V. Only if this process had happened, the fingerprint of distinct surface facets such as in Figure 3 can develop in acidic solution. Interestingly, NPG films made by free corrosion of a AgAu alloy film in HNO_3 by Wang at al.[23] restructured during cycling in 0.1 M H_2SO_4. The mole fraction x(Ag) as measured by XPS decreased from 1.5 % for the initial film after dealloying to 0.6 % and 0.8 % after potential cycling. Wang at al.[23] considered this effect as insignificant for electrocatalysis but did not comment on the role of residual silver in the restructuring process. By observing the cycling in KOH before and after one cycle in H_2SO_4, our finding provides insights into the role of the residual silver on top of the surface, acting as stabilizer of the high energetic curvature of ligaments, as proposed by TEM studies.[40]

3. Conclusions

Potential cycling of NPG in sulfuric acid solution causes the formation of low index crystal facets on the surface of the ligaments. According to SEM images, this process is *not* accompanied by coarsening of pores and ligaments. This observation suggests that electrochemical cycling changes the geometry of the ligaments form a more cylindrical shape with a high density of surface defects to a more prismatic shape with a similar size as the original ligament in the as dealloyed sample. In contrast, NPG does not show restructuring during potential cycling in potassium hydroxide solution. XPS results show that the surface Ag content increases during cycling in KOH and decreases during cycling in H_2SO_4. Taken together, the observation suggests that the electrolytic removal of residual Ag in acidic electrolytes is a prerequisite for the restructuring. The restructuring does not occur in alkaline media because Ag species remain linked to the surface and protect the surface defects from a restructuring to energetically more stable low index facets.

Experimental Section

Materials

Sulfuric acid 96 % (Suprapur®, Merk, Darmstadt, Germany), hydrochloric acid (Suprapur®, Merk, Darmstadt, Germany), and potassium hydroxide hydrate 99.995 % (Suprapur®, Merk, Darmstadt, Germany) were used as received. The solutions were made with ultrapure water (0.05 μS cm^{-1}). Argon 99.999 % (AlphagazTM) was used to purge the solution in the cell during at least 20 minutes, and the flow was maintained in the head space during the whole experiment to keep the inert atmosphere.

Procedures

Nanoporous gold samples were obtained from an $Ag_{75}Au_{25}$ master alloy. Therefore, Ag and Au wires (Ag ≥ 99.99 %, Au ≥ 99.99 %, Sigma Aldrich) were alloyed by arc melting in Ar atmosphere (MAM-1 E. Bühler) and homogenized in an evacuated quartz tube for 5 days at 850 °C (10^{-2} bar, RHF1600, Carbolite). Afterwards a wire of around 0.95 mm diameter was drawn and cut by a diamond saw (Model 3032-4, Well) into cylinders of 1.9 mm length. For healing defects introduced by the mechanical treatment, the samples were annealed in an evacuated furnace at 650 °C for 3 h (Mila-5000, Ulvac-Rico). For dealloying, the $Ag_{75}Au_{25}$ precursor was mounted in a three-electrode cell as working electrode, with a Ag wire as auxiliary electrode and a Ag/AgCl as reference electrode (both made from (> 99.99 % Ag wire, Sigma-Aldrich) in 1 M $HClO_4$ (prepared from 70 % $HClO_4$ Emsure, Merck and ultrapure water with 18.2 MΩ cm). The sample was oxidized potentiostatically (PGSTAT Autolab-Metrohm) at 1.25 V vs. SHE until the current dropped to 15 μA. Then, the potential was incremented to 1.35 V and held until the current had decayed to 15 μA. Subsequently, the sample was

cleaned by potentiodynamically cycling 20 times between 0.1 V and 1.6 V in 1 M $HClO_4$ at 5 mV s^{-1} followed by keeping the potential at 1.35 V for 20 min. Finally, the sample was cycled 20 times at 5 mV s^{-1} between 0.1 V and 1.6 V in fresh 1 M $HClO_4$ ending at 0.8 V. Afterwards, the sample was rinsed in ultrapure water and dried in air. The NPG samples had an average ligament diameter of 40 nm, a specific surface area of 11.8 $m^2 g^{-1}$, and a density of 4.99 g cm^{-3}. The residual Ag mole fraction $x(Ag) = 1\%$ was determined by EDX. We refer to this procedure as potentiodynamically controlled dealloying (PCD). The sample were stored in air and further used within 6 weeks. To obtain the powder, the dealloyed monolith was sonicated in a clean vial for 5 min and then triturated in an agate mortar until no appreciable changes in the grain size were visible. The material thus obtained is called here "as dealloyed". The powder was used for a period of 6 month after preparation.

Cavity microelectrodes (CME) were produced by sealing 1.5 cm gold wire of 100 μm diameter (99.99 + %, Goodfellow, Friedberg, Germany) in a borosilicate glass capillary. The assembly was grinded with grade 1200 abrasive paper using a EG-401 microgrinder (Narishige, Tokio, Japan) in order to expose the disk-shaped cross section of the Au wire. Subsequently, the Au wire inside the capillary was connected to a Cu wire with silver-epoxy glue (EPO-TEKs, John P. Kummer GmbH, Germany). The cavities were formed by dissolving a part of the embedded gold wire potentiostatically at + 1.1 V vs. SCE in 1 M HCl during 100 s yielding cavities of (30 ± 2) μm depth. The quality of polishing of the microelectrodes and the depth of the cavities was assessed using a confocal laser scanning microscope (Leica TCS SP2, Leica Microsystems GmbH, Germany) equipped with a HC PL Fluotar 50x/0.8 dry lens. The obtained CME is immersed in piranha solution for at least 1 h before use. *For risk statement, see end of next paragraph.* Prior to each experiment, the cavity was washed with ultrapure water in an ultrasonic bath for 300 s. The cavity was filled by slightly pressing the CME into NPG powder. The end of the filled CME was washed with ultrapure water and the excess of NPG powder outside the cavity was wiped off with a soft cloth. The filling is monitored by inspection with an optical microscope in reflection mode at 20x magnification.

Electrochemical experiments were performed with an Autolab potentiostat PGSTAT128N (Metrohm, Filderstadt, Germany) equipped with an analog scan generator scan250 and NOVA 2.1 software. A cavity microelectrode was used as working electrode with an Au coil as auxiliary electrode and a $Hg/HgSO_4/K_2SO_{4(Sat)}$ reference electrode (ALS, Tokyo, Japan) in acid media free of Cl^- ions. A saturated calomel electrode (SCE) from ALS was used for etching the Au wire of the CME in acid media with Cl^- ions, and a Hg/HgO/1 M NaOH reference electrode from (ALS) was utilized in alkaline media. For the preparation of the CME, a Pt wire is used as auxiliary electrode for. All potentials are reported versus the reversible hydrogen electrode (RHE), converting the scale by means of the equation $E_{RHE} = E_{SHE} + 0.059\,V$ * pH, where $E_{SHE} = E(Hg|Hg_2SO_4|K_2SO_4\ (sat.)) + 0.640\,V$ and $E_{SHE} = E(Hg|HgO|1\ M\ NaOH) + 0.140\,V$. The pH of 0.1 M H_2SO_4 is taken as 1 and of 0.1 M KOH as 13 based on the average of 10 repetitive measurements. The electrochemical cell was mounted in a 25 mL-glass vial using a Teflon® cap with five necks. All glassware and electrodes were cleaned by immersion in 1 g/L $KMnO_4$ solution acidified with 20 mL/L solution of 96% (*m*/*m*) H_2SO_4 for at least 24 h. Subsequently, it was submerged in 40 mL 30% H_2O_2 solution acidified with 20 mL/L solution of 96% (*m*/*m*) H_2SO_4 and boiled once. *Caution: This mixture reacts violently with all organic materials. The solution has to be handled with extreme care to avoid personnel injury and property damage.* Finally, the excess of solution was removed by rinsing with ultrapure water and boiling three times.

The characterization of grain size and nanoporous structure was made with a scanning electron microscope (Helios Nanolab 600i system, FEI Company) equipped with an EDX detector using a 15 kV of acceleration voltage and a working distance of around 4 mm. The composition of NPG was characterized by XPS (ESCALAB 250Xi, Thermo Fisher Scientific, East Grinstead, UK) working with an Al Kα monochromatized X-ray source. The survey spectra were taken with a pass energy of 200 eV and energy step size of 1 eV. For high resolution analysis, the pass energy was 10 eV and energy step size was 0.02 eV.

Acknowledgements

The authors thank Deutsche Forschungsgemeinschaft for funding within the Research Group FOR2213-255613253 [subprojects 3 and 4]. Furthermore, funding is acknowledged for the SEM for the central facilities of the School of Mathematics and Science by the DFG (INST 184/107-1 FUGG) and for XPS instrumentation (INST 184/144-1 FUGG). Open access funding enabled and organized by Projekt DEAL.

Conflict of Interest

The authors declare no conflict of interest.

Keywords: nanoporous gold · coarsening · restructuring · electrochemical cycling · electrocatalysis

[1] a) A. Wittstock, A. Wichmann, M. Bäumer, *ACS Catal.* **2012**, *2*, 2199; b) A. Wittstock, V. Zielasek, J. Biener, C. M. Friend, M. Bäumer, *Science* **2010**, *327*, 319.
[2] R. Zeis, T. Lei, K. Sieradzki, J. Snyder, J. Erlebacher, *J. Catal.* **2008**, *253*, 132.
[3] L. P. Hernández-Saravia, A. Sukeri, M. Bertotti, *Int. J. Hydrogen Energy* **2019**, *44*, 15001.
[4] T. Fujita, T. Tokunaga, L. Zhang, D. Li, L. Chen, S. Arai, Y. Yamamoto, A. Hirata, N. Tanaka, Y. Ding, et al., *Nano Lett.* **2014**, *14*, 1172.
[5] C. Yu, F. Jia, Z. Ai, L. Zhang, *Chem. Mater.* **2007**, *19*, 6065.
[6] M. Graf, M. Haensch, J. Carstens, G. Wittstock, J. Weissmüller, *Nanoscale* **2017**, *9*, 17839.
[7] a) J. Weissmüller, R. C. Newman, H.-J. Jin, A. M. Hodge, J. W. Kysar, *MRS Bull.* **2009**, *34*, 577; b) A. Wittstock, J. Biener, M. Bäumer, *RSC Nanosci. Nanotechnol.* **2012**, *22*, 1.
[8] a) L. Zhang, L. Chen, H. Liu, Y. Hou, A. Hirata, T. Fujita, M. Chen, *J. Phys. Chem. C* **2011**, *115*, 19583; b) A. Lackmann, M. Bäumer, G. Wittstock, A. Wittstock, *Nanoscale* **2018**, *10*, 17166.
[9] C. Mahr, P. Kundu, A. Lackmann, D. Zanaga, K. Thiel, M. Schowalter, M. Schwan, S. Bals, A. Wittstock, A. Rosenauer, *J. Catal.* **2017**, *352*, 52.
[10] T. Krekeler, A. V. Straßer, M. Graf, K. Wang, C. Hartig, M. Ritter, J. Weissmüller, *Mater. Res. Lett.* **2017**, *5*, 314.
[11] a) A. Y. Chen, S. S. Shi, F. Liu, Y. Wang, X. Li, J. F. Gu, X. F. Xie, *Appl. Surf. Sci.* **2015**, *355*, 133; b) S. Kuwano-Nakatani, T. Fujita, K. Uchisawa, D. Umetsu, Y. Kase, Y. Kowata, K. Chiba, T. Tokunaga, S. Arai, Y. Yamamoto, et al., *Mater. Trans.* **2015**, *56*, 468.
[12] M. Hakamada, M. Mabuchi, *J. Mater. Res.* **2009**, *24*, 301.
[13] M. Graf, B. Roschning, J. Weissmüller, *J. Electrochem. Soc.* **2017**, *164*, C194–C200.
[14] N. Mameka, K. Wang, J. Markmann, E. T. Lilleodden, J. Weissmüller, *Mater. Res. Lett.* **2016**, *4*, 27.
[15] L.-Z. Liu, X.-L. Ye, H.-J. Jin, *Acta Mater.* **2016**, *118*, 77.
[16] A. Dursun, D. V. Pugh, S. G. Corcoran, *J. Electrochem. Soc.* **2003**, *150*, B355–B360.

[17] a) C. Lakshmanan, R. N. Viswanath, R. Rajaraman, S. Dash, G. Amarendra, C. S. Sundar, *Europhys. Lett.* **2017**, *117*, 48007/1–5; b) T. S. Dorofeeva, E. Seker, *Nanoscale* **2016**, *8*, 19551.
[18] M. Haensch, M. Graf, W. Wang, A. Nefedov, C. Wöll, J. Weissmüller, G. Wittstock, *ACS Appl. Nano Mater.* **2020**, *3*, 2197.
[19] T. S. Dorofeeva, Z. Matharu, P. Daggumati, E. Seker, *J. Phys. Chem. C* **2016**, *120*, 4080.
[20] Z. Matharu, P. Daggumati, L. Wang, T. S. Dorofeeva, Z. Li, E. Seker, *ACS Appl. Mater. Interfaces* **2017**, *9*, 12959.
[21] J. Snyder, P. Asanithi, A. B. Dalton, J. Erlebacher, *Adv. Mater.* **2008**, *20*, 4883.
[22] A. Sharma, J. K. Bhattarai, A. J. Alla, A. V. Demchenko, K. J. Stine, *Nanotechnology* **2015**, *26*, 85602/1–11.
[23] Z. Wang, S. Ning, P. Liu, Y. Ding, A. Hirata, T. Fujita, M. Chen, *Adv. Mater.* **2017**, *29*, 1703601/1–7.
[24] O. M. Magnussen, W. Polewska, L. Zitzler, R. J. Behm, *Faraday Discuss.* **2002**, *121*, 43.
[25] P. Ahrens, M. Zander, U. Hasse, H. Wulff, C. Jeyabharathi, A. Kruth, F. Scholz, *ChemElectroChem* **2018**, *5*, 943.
[26] C. Cachet-Vivier, M. Keddam, V. Vivier, L. T. Yu, *J. Electroanal. Chem.* **2013**, *688*, 12.
[27] G. Tremiliosi-Filho, L. H. Dall'Antonia, G. Jerkiewicz, *J. Electroanal. Chem.* **1997**, *422*, 149.
[28] a) N. Mameka, J. Markmann, H.-J. Jin, J. Weissmüller, *Acta Mater.* **2014**, *76*, 272; b) N. Mameka, J. Markmann, J. Weissmüller, *Nat. Commun.* **2017**, *8*, 1976; c) L. Lührs, B. Zandersons, N. Huber, J. Weissmüller, *Nano Lett.* **2017**, *17*, 6258.
[29] P. Ahrens, M. Zander, D. Hirsch, U. Hasse, H. Wulff, F. Frost, F. Scholz, *J. Electroanal. Chem.* **2019**, *832*, 233.
[30] A. A. Mikhri, A. G. Pshchenichnikov, P. K. Burshtein, *Elektrokhimiya* **1972**, *8*, 364.
[31] A. Hamelin, *J. Electroanal. Chem.* **1996**, *407*, 1.
[32] Z. Borkowska, A. Tymosiak-Zielinska, G. Shul, *Electrochim. Acta* **2004**, *49*, 1209.
[33] a) L. D. Burke, P. F. Nugent, *Gold Bull.* **1997**, *30*, 43; b) S. Cherevko, A. R. Zeradjanin, G. P. Keeley, K. J. J. Mayrhofer, *J. Electrochem. Soc.* **2014**, *161*, H822–H830; c) P. Quaino, N. B. Luque, R. Nazmutdinov, E. Santos, W. Schmickler, *Angew. Chem. Int. Ed.* **2012**, *51*, 12997; d) A. Hamelin, M. J. Sottomayor, F. Silva, S.-C. Chang, M. J. Weaver, *J. Electroanal. Chem.* **1990**, *295*, 291.
[34] J. Hernández, J. Solla-Gullón, E. Herrero, A. Aldaz, J. M. Feliu, *Electrochim. Acta* **2006**, *52*, 1662.
[35] a) J. Hernandez, J. Solla-Gullón, E. Herrero, A. Aldaz, J. M. Feliu, *J. Phys. Chem. B* **2005**, *109*, 12651; b) J. Hernandez, J. Solla-Gullón, E. Herrero, *J. Electroanal. Chem.* **2004**, *574*, 185; c) J. Hernandez, J. Solla-Gullon, E. Herrero, J. M. Feliu, A. Aldaz, *J. Nanosci. Nanotechnol.* **2009**, *9*, 2256.
[36] S. Cherevko, A. A. Topalov, A. R. Zeradjanin, I. Katsounaros, K. J. J. Mayrhofer, *RSC Adv.* **2013**, *3*, 16516.
[37] J. M. M. Droog, P. T. Alderliesten, G. A. Bootsma, *J. Electroanal. Chem. Interfacial Electrochem.* **1979**, *99*, 173.
[38] M. Schalenbach, O. Kasian, M. Ledendecker, F. D. Speck, A. M. Mingers, K. J. J. Mayrhofer, S. Cherevko, *Electrocatalysis* **2018**, *9*, 153.
[39] S. Cherevko, C.-H. Chung, *Electrochem. Commun.* **2011**, *13*, 16.
[40] T. Fujita, P. Guan, K. McKenna, X. Lang, A. Hirata, L. Zhang, T. Tokunaga, S. Arai, Y. Yamamoto, N. Tanaka, et al., *Nat. Mater.* **2012**, *11*, 775.

Manuscript received: July 13, 2020
Revised manuscript received: August 20, 2020
Accepted manuscript online: August 25, 2020